Modeling Radial-Flow Ion-Exchange Bed Performance

Hai M. Duong and David C. Shallcross*

Department of Chemical and Biomolecular Engineering, University of Melbourne, Victoria 3010, Australia

A theoretical model is developed that predicts the performance of an annular ion-exchange bed involving the exchange of two cations. In the model, the solution to be treated is assumed to flow radially through the fixed bed either away from the bed's axis or toward it. Unlike an earlier model, this model does not assume that an instantaneous equilibrium exists between the two phases. The model incorporates mass-transfer terms including film diffusion and solution-phase phenomena. The exchange phase is assumed to consist of randomly packed synthetic and spherical resin beads of a narrow size range. The binary equilibrium relationship is characterized by a form of the Langmuir equation. The model permits the performance of an ion-exchange bed to be predicted. Breakthrough times and composition profiles within the bed may also be calculated. The model is validated by comparing its predictions with those made by a purpose-built annular ion-exchange bed. The performance of the radial bed is studied for both the exhaustion and regeneration cycles for the Na^+-H^+ and $Ca^{2+}-H^+$ cation binary systems. Using the validated radial-flow model, the ion-exchange performances of a nonlinear (radial) bed under different operating conditions are also studied.

Introduction

In the radial-flow ion-exchange process, the solution to be treated passes in the radial direction through an annular ion-exchange bed. In one possible implementation of the process, the solution is injected at the inner face of the annular bed and then flows outward away from the bed's axis, with the effluent being collected at the bed's periphery. Radial-flow ion exchange offers a number of advantages over the more conventional ion-exchange process involving linear flow through a cylindrical bed. The depth of a commercial and conventional ion-exchange bed is usually limited by the mechanical strength of the ion-exchange medium, often a resin bead. Because the beads at the bottom of the bed must be able to withstand the forces acting down on them including the weight of the bed above, the depth of the bed may be limited to just 1 m. Obviously, the permissible depth of the bed might be increased to a limited extent by limiting the throughput. In an annular ion-exchange bed, the path length through the bed is governed by the outer and inner diameters of the bed and not its height. It may, therefore, be possible to increase the path length that the solution travels through the bed by simply increasing the bed diameter. The constraint on the path length would then be the maximum outer diameter that a large radial bed could be constructed with.

The large-scale application of the radial-flow ion-exchange process was first developed in Europe in the 1980s, but the technology was not developed commercially. The technology was later taken up in the U.S. when a patent was granted for the removal of groundwater contaminants and the treatment of wastewater and industrial effluents by the use of an ion-exchange medium packed in a radial-flow column.[1]

The linear ion-exchange processes within the column have been well studied by several workers.[2−4] Tsaur and Shallcross[5,6] proposed the first theoretical model for predicting the performance of the radial-flow ion-exchange process. Their model showed that under certain operating conditions the performance of a radial-flow ion-exchange bed was superior to that of a conventional cylindrical bed. Their model assumed, however, that instantaneous equilibrium between ions in the solution and exchanger phases existed throughout the exchanger. The model ignored the mass-transfer phenomena existing within the bed. The aim of this current work is to extend the model of Tsaur and Shallcross by incorporating mass-transfer effects. As well as improving the reliability of the model predictions, this new model would be a more valuable design tool.

Rachinskii[7] applied the equilibrium theory in the theoretical study of radial chromatography. In modeling ion-exchange performances in an annular resin bed, he made two simplifications: ideal ion exchange with a linear equilibrium relation and no dispersion in the radial-flow direction. Hang et al.[8] modified the Rachinskii model[7] by taking into account the dispersion effect and stated that the comparisons of simulations between radial and axial chromatography and also the model equation itself show that if dispersion is neglected, radial and axial chromatography cannot be distinguished. Rice and Heft[9] conducted radial chromatography experiments in a pancake-shaped bed to test the predictions by the modified Rachinskii model.[7] Their works show that the model prediction agrees well with the experimental data and also suggest that radial dispersion controls the breakthrough curve broadening. The model validation is only for paper or thin- and small-layer chromatography.

Simple dispersion in porous media in radial-flow geometry has been studied. Most work performed related to theoretical studies on the instability of displacement within porous media in radial flow. Tan and Homsy[10] proposed a model based on the assumption of a constant dispersion coefficient in cylindrical coordinates for isotropic dispersion in the radial direction. Yortsos[11] improved Tan and Homsy's model[10] by con-

* To whom correspondence should be addressed. Tel.: +61 3 8344 6614. Fax: +61 3 8344 4153. E-mail: dcshal@unimelb.edu.au.

10.1021/ie048941y CCC: $30.25
Published on Web 03/25/2005

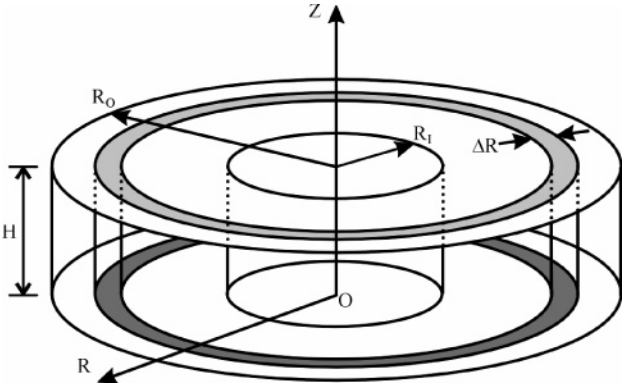

Figure 1. Representation of a fixed annular ion-exchange bed of constant thickness, H, showing the annular element.

sidering anisotropic dispersion. Zimmerman and Homsy[12] modified the Yortsos model by applying the radial dispersion coefficient as a function of the radial pore velocity. They solved their dispersion model numerically and applied model predictions in a study on stabilities of displacement in radial flow through porous media.

In this study, a mathematical model is developed to predict the ion-exchange performance in an annular ion-exchange bed. By incorporation of mass-transfer effects and by the elimination of the assumption of instantaneous equilibrium throughout the bed, the model is a significant improvement over that proposed by Tsaur and Shallcross.[5] The radial-flow ion-exchange model predictions are tested by comparing them with the observations made during experiments in a radial, wedge-shaped bed. Using the validated radial-flow model, computer simulations are performed to study the ion-exchange performances of an annular radial-flow ion-exchange bed under different operating conditions, including different bed porosities, different bed geometries, different exchanger resin bead sizes, different flow rates, different injected solution concentrations, and different flow directions.

Radial-Flow Ion-Exchange Model

The model considers the binary ion-exchange processes within an annular bed of constant thickness H, inner radius R_I, and outer radius R_O (Figure 1). The fixed, homogeneous bed is assumed to be made up of randomly packed spherical beads all having the same diameter. Flow through the bed is assumed to be one-dimensional in the radial direction. In such a bed, the bed cross-sectional area perpendicular to flow is a function of the radial position, increasing away from the bed's axis. The bed porosity, ϵ_b, is assumed to be uniform throughout the bed.

Flow through the bed may be outward from the inner face at R_I to the outer face at R_O (diverging flow) or inward from the outer face to the inner face (converging flow). We will illustrate the development of the following model by assuming the flow is outward, away from the bed's axis.

Within the system, it is assumed that only two exchanging species are present, namely, A and B. For the purposes of illustration, we will assume that these are cations. It should be noted, however, that the model is equally applicable to anion exchange.

Initially, the exchanger bed is completely in the B form (i.e., all of the exchange sites on exchanger beads are occupied by B cations), and the only cations present in the solution phase within the pores of the exchanger bed are of species B. Cations of species A are absent from the bed. At some time $\tau = 0$ and thereafter, a solution containing A cations at a known and constant concentration is injected into the inner face of the bed. The solution is injected at a volumetric flow rate, F_L, that is both uniform over the entire inner face of the bed and constant with time. At the same time, an effluent solution is produced from the outer face of the exchanger bed. This effluent solution is produced at a rate that is assumed to be constant and uniform over the entire outer face. For diverging flow, the velocity of the solution passing through the bed slows as it moves away from the bed's axis.

As with exchanger beds of conventional design, for some time after injection of the A solution begins, no A cations appear in the effluent solution. In that part of the bed near the inner face of the bed, ion exchange occurs, with the A cations in the solution exchanging with the B cations on the exchanger according to the equation

$$a\underline{B}^{b+} + b\underline{A}^{a+} \leftrightarrow bA^{a+} + aB^{b+} \quad (1)$$

where a and b are the valencies of A and B, respectively, and the underline indicates that the particular species is in the exchanger phase rather than the solution phase. As the exchanger sites near the inner face progressively fill with A cations in exchange for B cations, the concentration of A cations in the effluent solution gradually rises until the effluent concentration has reached that of the injected solution. In designing and operating the exchanger, we need to be able to predict the breakthrough time for the system, i.e., the time at which the exchanging cation A first appears at significant levels in the effluent.

Tsaur and Shallcross[5] developed a model to predict the binary ion-exchanger performance of such an annular exchange bed. Their model assumed that equilibrium between the ions in the solution and exchanger phases was established instantaneously throughout the entire bed. The model proposed in this paper eliminates this assumption and considers mass-transfer effects within the porous bed.

Like the model proposed by Tsaur and Shallcross,[5] this model is based upon the material balance for A cations over an annular section of the bed having a thickness of ΔR between radial positions R and $R + \Delta R$. At some time $\tau > 0$, C_A will be the volumetric concentration of A cations in the solution phase within the section and C_{RA} will be the concentration of A cations in the exchanger phase also within the section. Both C_A and C_{RA} will vary with R. J_A is the dispersive flux of A ions through the elemental annular section. J_A is also a function of radial position R.

Tsaur and Shallcross showed that the cation concentrations in the two phases are related to the dispersive flux by

$$\frac{\partial C_A}{\partial \tau} + \left(\frac{1-\epsilon_b}{\epsilon_b}\right)\frac{\partial C_{RA}}{\partial \tau} = -\frac{\partial}{\partial R}(J_A) - \frac{F_L}{\epsilon_b A_R}\frac{\partial C_A}{\partial R} \quad (2)$$

In this equation, the terms on the left-hand side arise from the accumulation of A ions in the solution phase and in the resin phase. The first term on the right-hand side arises from the dispersion terms, while the second term results from the convective terms.

Using Fick's law to relate the dispersion flux in the radial direction to the concentration gradient in the cylindrical coordinates, we have

$$J_A = -D_{LR}\frac{\partial C_A}{\partial R} \tag{3}$$

where the dispersion coefficient, D_{LR}, is assumed to be independent of C_A but is assumed to be a function of the solution velocity through the porous resin bed:

$$D_{LR} = f(U_{RP}) \tag{4}$$

Here, U_R is the superficial velocity at the position R and U_{RP} is the pore velocity at the position R. Because the solution is injected at a constant flow rate and the resin bed has uniform porosity, we have

$$U_{RP} = \frac{U_R}{\epsilon_b} = \frac{F_L}{A_R\epsilon_b} = f(R) \tag{5}$$

In cylindrical coordinates, the derivative of the radial dispersion flux is

$$\frac{\partial}{\partial R}(J_A) = -\frac{1}{R}\frac{\partial}{\partial R}\left(RD_{LR}\frac{\partial C_A}{\partial R}\right) = -\left(D_{LR}\frac{\partial^2 C_A}{\partial R^2} + \frac{D_{LR}}{R}\frac{\partial^2 C_A}{\partial R} + \frac{\partial D_{LR}}{\partial R}\right) \tag{6}$$

Substitution of eq 6 into the balance equation of eq 2 yields

$$\frac{\partial C_A}{\partial \tau} + \left(\frac{1-\epsilon_b}{\epsilon_b}\right)\frac{\partial C_{RA}}{\partial \tau} = D_{LR}\frac{\partial^2 C_A}{\partial R^2} + \frac{D_{LR}}{R}\frac{\partial C_A}{\partial R} + \frac{\partial D_{LR}}{\partial R}\frac{\partial C_A}{\partial R} - \frac{F_L}{\epsilon_b A_R}\frac{\partial C_A}{\partial R} \tag{7}$$

The rate of change in the concentration of cation A in the resin phase may be given by

$$\frac{\partial C_{RA}}{\partial \tau} = \frac{a_s}{v}J_{RA} \tag{8}$$

where a_s and v are the surface area and volume of a spherical exchanger bead and J_{RA} is the flux of the cation A passing through the surface of the bead. Because the exchanger beads are assumed to be spherical, we may write

$$\frac{a_s}{v} = \frac{3}{R_c} \tag{9}$$

Here R_c is the radius of the exchanger bead. So

$$\frac{\partial C_{RA}}{\partial \tau} = \frac{3}{R_c}J_{SA} \tag{10}$$

For this work, we will assume that the kinetics of the ion-exchange process are controlled by the diffusion of the ions across a hydrostatic boundary layer (Nernst film) that surrounds the particles. This assumption is reasonable because the resin beads are relatively small and the concentration of the bulk solution is relatively low. This assumption implies that there is instantaneous transport of ions within the exchanger bead compared to the transport of ions across the Nernst film.

We shall further assume that there is a linear relationship between the flux and the concentration difference between the bead surface and the bulk phase. Thus

$$J_{RA} = k_f(C_A - C_{SA}) \tag{11}$$

where k_f is the mass-transfer coefficient for the liquid film and C_{SA} is the concentration of cation A in the solution phase but at the surface of the exchanger bead. Thus

$$\frac{\partial C_{RA}}{\partial \tau} = \frac{3}{R_c}k_f(C_A - C_{SA}) \tag{12}$$

If we assume that film diffusion is the rate-controlling step, then we may assume that the solution at the surface of the beads will be in equilibrium with the ions in the resin.

Equation 7 becomes

$$\frac{\partial C_{RA}}{\partial \tau} = D_{LR}\frac{\partial^2 C_A}{\partial R^2} + \frac{D_{LR}}{R}\frac{\partial C_A}{\partial R} + \frac{\partial D_{LR}}{\partial R}\frac{\partial C_A}{\partial R} - \frac{F_L}{\epsilon_b A_R}\frac{\partial C_A}{\partial R} - \left(\frac{1-\epsilon_b}{\epsilon_b}\right)\frac{3k_f}{R_c}(C_A - C_{SA}) \tag{13}$$

The concentration of A cations in the solution phase, C_A, may be written in terms of the solution phase cation mole fraction, x. Hence

$$C_A = xC_0 \tag{14}$$

where C_0 is the total normality in the solution. C_0 does not change when ionic species of differing valances exchange with one another.

Similarly, the concentration of A cations at the surface in the solution phase in equilibrium with the resin surface concentration, C_{SA}, may be written in terms of the mole fraction of A in the solution phase but at the surface of the exchanger bead, x_S:

$$C_{SA} = x_S C_0 \tag{15}$$

The concentration of cation species A in the solid resin phase, C_{RA}, may be written in terms of the solid resin phase mole fraction, y. This is defined as the fraction of the cations on the resin that are cation species A. Therefore

$$C_{RA} = yQ_c\rho_c \tag{16}$$

where Q_c is the cation-exchange capacity of the resin on a mass basis and ρ_c is the resin density.

As noted above, if we assume that film diffusion is the rate-controlling step, then we may assume that the solution at the surface of the beads will be in equilibrium with the ions in the exchanger phase. Thus, a relationship must exist between x_S and y:

$$x_S = f(y) \tag{17}$$

In their earlier study, Tsaur and Shallcross[5] applied a sophisticated and computationally intensive equilibrium

model developed by Mehablia et al.[13,14] to link the two phases. This equilibrium model takes into account the nonideal behavior in both the solution and exchanger phases and can easily respond to variations in solution concentrations. The incorporation of this type of equilibrium model increases by at least 1 order of magnitude the execution time of the computer program developed for the model.

Rather than use such a sophisticated model, in this study we link the mole fractions of the A cations at the exchanger surface in both phases, x_S and y, by the isotherm equation of the form

$$x_S = \frac{p_1 y^{p_2}}{p_3 + y^{p_2}} + \frac{p_4 y^{p_5}}{p_6 y^{p_5}} \tag{18}$$

where p_1-p_6 are empirical constants of the equilibrium isotherm equation obtained by fitting the equilibrium experiments. An equation of this form is chosen because it is able to adequately represent a range of equilibrium behavior. Values for the parameters p_1-p_6 may be fitted from the experimental data. The values vary from system to system and with varying solution concentrations.

Equation 13 may be expressed in terms of the mole fractions of A (i.e., x and x_S) rather than concentrations (i.e., C_A and C_{SA}):

$$\frac{\partial x}{\partial \tau} = D_{LR}\frac{\partial^2 x}{\partial R^2} + \frac{D_{LR}}{R}\frac{\partial x}{\partial R} + \frac{\partial D_{LR}}{\partial R}\frac{\partial x}{\partial R} - \frac{F_L}{\epsilon_b A_R}\frac{\partial x}{\partial R} - \frac{1-\epsilon_b}{\epsilon_b}\frac{3k_f}{R_c}(x - x_S) \tag{19}$$

When this equation is expressed in dimensionless form, the problem may more easily be solved. Define

$$r = R/R_0 \tag{20}$$

and

$$t = \frac{\tau F_L}{\epsilon_b A_{R_0} R_0} = \frac{\tau F_L}{\epsilon_b (2\pi) H R_0^2} \tag{21}$$

where r and t are the dimensionless radial position and time, respectively.

Substitution of r and t into eq 19 yields

$$\frac{F_L}{\epsilon_b (2\pi) R_0^2 H}\frac{\partial x}{\partial t} = \frac{D_{LR}}{R_0^2}\frac{\partial^2 x}{\partial r^2} + \frac{D_{LR}}{r R_0^2}\frac{\partial x}{\partial r} + \frac{1}{R_0}\frac{\partial D_{LR}}{\partial R}\frac{\partial x}{\partial r} - \frac{F_L}{\epsilon_b (2\pi) R_0 r H}\frac{1}{R_0}\frac{\partial x}{\partial R} - \left(\frac{1-\epsilon_b}{\epsilon_b}\right)\frac{3k_f}{R_c}(x - x_S) \tag{22}$$

Multiplying through by $2\pi\epsilon_b R_0^2 H/F_L$ yields

$$\frac{\partial x}{\partial \tau} = \frac{D_{LR}(2\pi)\epsilon_b H}{F_L}\frac{\partial^2 x}{\partial r^2} + \frac{D_{LR}(2\pi)\epsilon_b H}{F_L}\frac{1}{r}\frac{\partial x}{\partial r} + \frac{2\pi\epsilon_b H}{F_L} R_0 \frac{\partial D_{LR}}{\partial R}\frac{\partial x}{\partial r} - \frac{1}{r}\frac{\partial x}{\partial r} - \left(\frac{1-\epsilon_b}{\epsilon_b}\right)\frac{2\pi\epsilon_b R_0^2 H}{F_L}\frac{3k_f}{R_c}(x - x_S) \tag{23}$$

The Péclet number is defined as the ratio of the bulk mass transfer to dispersive transfer in the radial direction:

$$Pe_R = U_R R/D_{LR}\epsilon_b \tag{24}$$

Here, U_R is the superficial velocity given by

$$U_R = \frac{F_L}{A_R} = \frac{F_L}{2\pi R H} \tag{25}$$

Equation 23 may therefore be written as

$$\frac{\partial x}{\partial \tau} = \frac{1}{Pe_R}\frac{\partial^2 x}{\partial r^2} + \left(\frac{1}{Pe_R} - 1\right)\frac{1}{r}\frac{\partial x}{\partial r} + \frac{1}{Pe_R}\frac{R_0}{D_{LR}}\frac{\partial D_{LR}}{\partial R}\frac{\partial x}{\partial r} - \left(\frac{1-\epsilon_b}{\epsilon_b}\right)\frac{1}{Pe_R}\frac{R_0^2}{D_{LR}}\frac{3k_f}{R_c}(x - x_S) \tag{26}$$

This equation describes the one-dimensional radial-flow ion-exchange process within a fixed annular bed. The ion exchange occurs with radial dispersion and both ion exchange and radial dispersion develop with time.

It is useful to express eq 12 in a dimensionless form:

$$\frac{\partial y}{\partial t} = \frac{3k_f}{R_c}\frac{1}{Pe_R}\frac{R_0^2}{D_R}\frac{C_0}{Q_c \rho_c}(x - x_S) \tag{27}$$

The total exchange capacity of a complete annular bed, Q_{RT}, is given by

$$Q_{RT} = Q_c \rho_c (1-\epsilon_b)\pi(R_0^2 - R_1^2)H \tag{28}$$

Note that Q_{RT} may be evaluated by experiments.

Substitution of eq 28 into eq 27 yields

$$\frac{\partial y}{\partial t} = \frac{3k_f}{R_c}\frac{1}{Pe_R}\frac{R_0^2}{D_R}\frac{C_0}{Q_{RT}}(1-\epsilon_b)\frac{\pi(R_0^2 - R_1^2)H}{12}(x - x_S) \tag{29}$$

Equations 26 and 29 are the basis for the theoretical model for the cation-exchange processes within the radial-flow system. These equations may be solved to find the cation concentration in either phase at any time and radial position. The equations are not limited to considering exchange between just two cations but may also be applied to multicomponent ion-exchange processes. These equations may be numerically solved by the finite-difference technique.

The solution mole fraction at the exchanger surface in equilibrium with the resin phase mole fraction, x_S, is linked to the resin phase mole fraction, y, by eq 18. Substitution of eq 18 into eqs 26 and 29 yields two equations with only two variables of x and y. These equations may then be solved simultaneously.

Several assumptions are implicit in the development of the model equations:

(1) The resin bed is homogeneous with uniform porosity.

(2) The resin bed has finite outer and inner radii.

(3) The resin beads are spherical and all of the same size.

(4) The resin bed is fixed and does not move.

(5) Both fluid and resin bead compressibilities are negligible, and gravity effects are neglected.

(6) Fluid flows at a rate that is constant with time and uniform throughout the resin bed. The flow is isothermal.

(7) Molecular diffusion is negligible.

(8) Dispersion occurs only in the flow direction and is isotropic for the same radius.

(9) The dispersion coefficient is independent of the chemical concentration but is a function of the radial distance.

(10) Film diffusion is the rate-controlling step for the ion-exchange process.

(11) The temperature is constant and uniform within the system.

(12) The physical properties of the solution, such as density and viscosity, may be approximated by those of water.

Because the cation resin beads are initially in the B form and the solution within the pores of the bed contains no A cations, then the initial conditions for the system are

$$x = 0 \qquad \text{at } t = 0 \qquad \text{for } r_I \le r \le r_O \tag{30a}$$

$$y = 0 \qquad \text{at } t = 0 \qquad \text{for } r_I \le r \le r_O \tag{30b}$$

At $t = 0$, there is a step change in the composition and concentration of the solution injected into the bed. Thereafter, the composition and concentration remain constant. The boundary condition at the outlet for the cation concentration should be of the form $\partial^n x/\partial r^n = 0$, where n is the order of the derivative. The second-order derivative is chosen because higher order derivatives would unnecessarily complicate the model, while using the first-order derivative would be physically inappropriate and would significantly distort the model predictions at the outlet. Thus, the boundary conditions for the system are

$$x = 1 \qquad \text{at } r = r_I \qquad \text{for } t > 0 \tag{31a}$$

$$\frac{\partial^2 x}{\partial r^2} = 0 \qquad \text{at } r = r_0 \qquad \text{for } t > 0 \tag{31b}$$

The model equations are solved using an explicit finite-difference technique. In the solution of the finite-difference versions of the model equations, the radial distance between the inner and outer annular faces is divided into 201 equally spaced nodes. Further details of the numerical solution techniques employed are presented by Duong.[15]

Comparisons of the Radial-Flow Ion-Exchange Models

The original experimental data of Tsaur[16] is used in order to compare the accuracies of the predictions made by our model with those of Tsaur and Shallcross.[5] Tsaur studied the ion-exchange performance of a wedge-shaped resin bed for both the exhaustion and regeneration cycles for the Na^+-H^+ and $Ca^{2+}-H^+$ cation binary systems.

Experiments to validate the model were conducted by Tsaur[16] using a wedge-shaped cell having 30° of arc and containing Dowex MSC-1 resin. The resin used in Tsaur's work is Dowex, a macroporous polystyrene–divinylbenzene resin with active sulfonated groups. The radial ion-exchange cell consists of a wedge-shaped ion-exchange resin bed. The bed is formed from two parallel and horizontal Perspex sheets 15.0 mm apart. The two side walls are perpendicular to the two sheets but at an angle of 30° to one another. The radius of the inner curved wall is 30.0 mm, while the radius of the outer curved wall is 300.0 mm. Eleven identical chambers are distributed uniformly along the length of the outer face of the outer curved glass sheet. Each chamber is connected to flow lines of identical lengths that then pass to a multichannel peristaltic pump. All material, the wedge-shaped cell apparatus, and experimental procedures are described more fully by Tsaur.[16]

Table 1. Equilibrium Isotherm Equations for the Na^+-H^+ and $Ca^{2+}-H^+$ Cation Binary Systems

binary system	concn (N)	equilibrium isotherm equation
Na^+-H^+	0.10	$x_{Ca} = \dfrac{0.92y_{Ca}^{1.98}}{0.50 + y_{Ca}^{1.98}} + \dfrac{0.40y_{Ca}^{6.42}}{0.23 + y_{Ca}^{6.42}}$
		$x_H = 1 - \dfrac{0.92y(1-y_H)^{1.98}}{0.50 + (1-y_H)^{1.98}} - \dfrac{0.45(1-y_H)^{6.42}}{0.23(1-y_H)^{6.42}}$
	0.50	$x_{Ca} = \dfrac{1.63(1-y_H)^{1.33}}{1.50 + (1-y_H)^{1.33}} + \dfrac{0.42y_{Ca}^{5.50}}{0.21 + y_{Ca}^{5.50}}$
		$x_H = 1 - \dfrac{1.63(1-y_H)^{1.33}}{1.50 + (1-y_H)^{1.33}} - \dfrac{0.42(1-y_H)^{5.50}}{0.21 + (1-y_H)^{5.50}}$
$Ca^{2+}-H^+$	0.10	$x_{Ca} = \dfrac{3.92y_{Ca}^{10.94}}{6.03 + y_{Ca}^{10.94}} + \dfrac{4.85y_{Ca}^{11.89}}{2.05 + y_{Ca}^{11.89}}$
		$x_H = 1 + \dfrac{3.92(1-y_H)^{10.94}}{6.03 + (1-y_H)^{10.94}} - \dfrac{4.85(1-y_H)^{11.89}}{2.05 + (1-y_H)^{11.89}}$
	0.50	$x_{Ca} = \dfrac{0.33y_{Ca}^{7.44}}{0.08 + y_{Ca}^{7.44}} + \dfrac{0.86y_{Ca}^{14.25}}{0.21 + y_{Ca}^{14.25}}$
		$x_H = 1 - \dfrac{0.33(1-y_H)^{7.44}}{0.08 + (1-y_H)^{7.44}} - \dfrac{0.86(1-y_H)^{14.25}}{0.21(1-y_H)^{14.25}}$

Table 2. Summary of the Dispersion Experiment Performance in the Wedge-Shaped Resin Bed

resin bed		flow rate	dispersion coefficient	dispersion
form	porosity	(mL/h)	(cm^2/min)	length (cm)
Na	0.330	410	$0.005U_{RP}$	0.005
		1014	$0.008U_{RP}$	0.008
H	0.310	408	$0.009U_{RP}$	0.009
		1010	$0.013U_{RP}$	0.013

The equilibrium behaviors of the Na^+-H^+ and $Ca^{2+}-H^+$ binary ion-exchange systems were studied experimentally using a batch technique. These two systems were chosen to represent 1–1 and 1–2 valance systems. In both systems, chloride was the only anion present. Table 1 presents the binary isotherm equations derived for Tsaur's experimental equilibrium data.

For axial dispersion determination, a series of tracer experiments were conducted by Tsaur to determine the dispersion coefficients within the radial ion-exchange bed. The dispersion experiments performed in the wedge-shaped cell for both the Na-form bed and the H-form bed at two different flow rates are summarized in Table 2. Because the cross-sectional area of the resin bed in the wedge-shaped cell is not a constant but varies with the radial distance from the central inlet, the pore velocity is a function of the radial distance. Consequently, the pore velocity dependent dispersion coefficient is also a function of the radial distance.

Tsaur[16] conducted a series of experiments involving the exhaustion and regeneration of the ion-exchange bed for both binary systems. System flow rates and concentrations were also varied. The experiments conducted by Tsaur in the wedge-shaped bed are summarized in Table 3.

Table 3. Summary of the Wedge-Shaped Resin Bed Ion-Exchange Performance Experiments Conducted by Tsaur[16]

operation cycle	resin bed form	injection solution	solution concn (N)	flow rate (mL/h)	no. of data points
regeneration	Na	HCl	0.530	388	27
exhaustion	H	NaCl	0.500	393	19
regeneration	Na	HCl	0.530	393	22
exhaustion	H	NaCl	0.500	385	18
regeneration	Na	HCl	0.530	947	28
exhaustion	H	NaCl	0.250	975	25
regeneration	Ca	HCl	0.530	385	20
exhaustion	H	$CaCl_2$	0.500	376	13
regeneration	Ca	HCl	0.530	380	21
exhaustion	H	$CaCl_2$	0.500	378	12
regeneration	Ca	HCl	0.530	989	20
exhaustion	H	$CaCl_2$	0.250	936	21

Figures 2−5 allow comparisons to be made graphically between the breakthrough curves obtained by Tsaur's experiments and the breakthrough curves predicted using Tsaur's model and the model presented here. The reader should recall that the main difference between the two models is that Tsaur and Shallcross[5,6] assumed that instantaneous equilibrium existed between the ions in the solution and exchanger phases throughout the ion-exchange bed while the model proposed here does not make this assumption and instead considers the rate of the exchange process to be controlled by film diffusion.

For each system investigated and presented in Figures 2−5, the experiments were conducted twice. It may be seen that the experiments were very reproducible. The experimental errors are estimated to be less than 0.5%.

The weighted relative residue $\mathscr{R}$ is used to quantify the agreement between the breakthrough curves obtained by Tsaur's experiments and the theoretical models. The smaller the relative residue $\mathscr{R}$, the better the predictions made by the model. The weighted relative residue may be defined as

$$\mathscr{R} = \frac{\sum_{i=1}^{N} \left| \frac{V_{i,\text{predict}} - V_{i,\text{experiment}}}{V_{i,\text{predict}}} \right| W_i}{N-1} \tag{32}$$

For a given mole fraction of the contaminating ion in the effluent, $V_{i,\text{predict}}$ and $V_{i,\text{experiment}}$ are the effluent volume predicted by the model and measured in the experiments, respectively, N is a number of experimental data points, and W_i is the value of the weighting function. The weighting function may be calculated by

$$W_i = 1 - e^{-kx_i(1-x_i)} \tag{33}$$

where x_i is the mole fraction in the effluent and k is the penal power of the weighting function. k determines the shape of the weighting function.

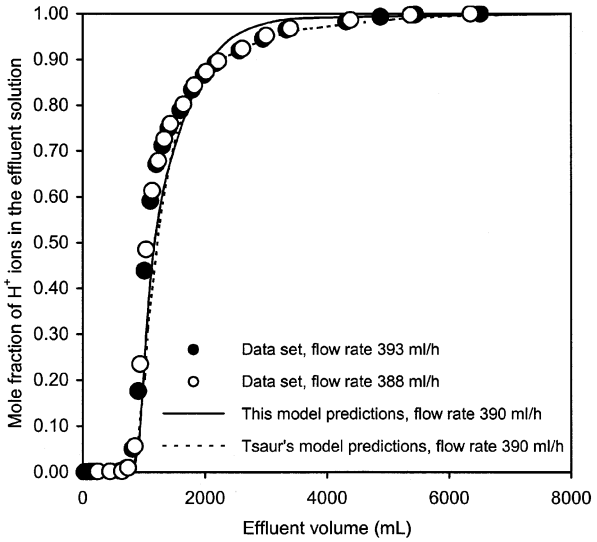

Figure 2. Breakthrough curves for the Na−H regeneration runs using a 0.53 N HCl solution at a flow rate of 390 mL/h. Wedge-shaped cell resin bed initially in the Na form.

This weighting function is used because it favors the more reliable central data at the expense of the less reliable data measured at the extreme ends of the composition ranges. A value for k of 10 is used. The weighting factor approaches zero when x_i approaches either 0 or 1. The values of the weighted relative residue $\mathscr{R}$ calculated by the proposed model and those of the Tsaur and Shallcross[5] model are summarized in Table 4. In all cases, we see that the predictions of the proposed model are superior to those of Tsaur and Shallcross.[5] The improvement in the predictions is pronounced for the higher flow rates.

Figure 2 presents the breakthrough curves for the regeneration when a 0.53 N HCl solution is drawn through the bed. In the first experiment, the solution is drawn at a flow rate of 388 mL/h, while in the second experiment, the solution is drawn at the slightly higher flow rate of 393 mL/h. Tsaur's and the developed models use an average flow rate of 390 mL/h. As may be seen by comparing the results from the two separate experiments, the data are reproducible. The agreement in Figure 2 between the experimental observations and the model prediction is very good except for the deviation at breakthrough between 1000.0 and 1500.0 mL of effluent volume. In comparison with the Tsaur model in terms of the weighted relative residue listed in Table 4, the proposed model gives a slightly better prediction.

The breakthrough curves for Na−H exhaustion runs are shown in Figure 3 when a 0.50 N NaCl solution is drawn through the resin bed initially in the H form. In

Table 4. Summary of the Weighted Relative Residue Calculated by the Proposed Model and Tsaur's Model

operation cycle	resin bed form	injection solution	flow rate (mL/h)	no. of data points	weighted relative residue: proposed model	weighted relative residue: Tsaur's model
regeneration	Na	0.530 N HCl	390	49	0.060	0.061
exhaustion	H	0.500 N NaCl	389	37	0.028	0.034
regeneration	Na	0.530 N HCl	947	28	0.015	0.081
exhaustion	H	0.250 N NaCl	975	25	0.024	0.035
regeneration	Ca	0.530 N HCl	383	41	0.064	0.102
exhaustion	H	0.500 N $CaCl_2$	377	25	0.030	0.040
regeneration	Ca	0.530 N HCl	989	20	0.067	0.082
exhaustion	H	0.250 N $CaCl_2$	936	21	0.027	0.084

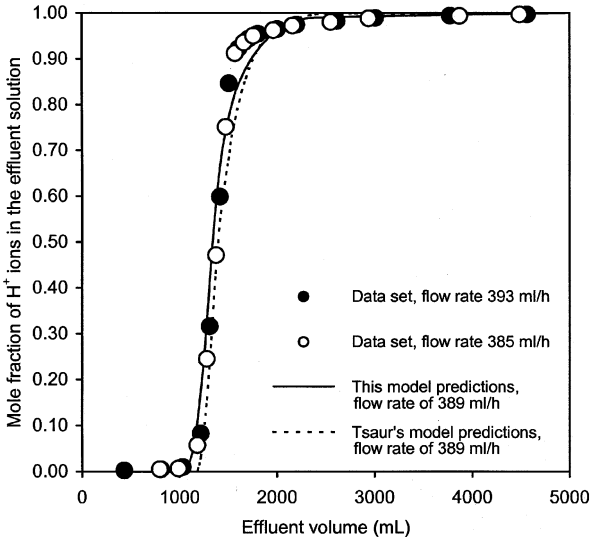

Figure 3. Breakthrough curves for the Na−H exhaustion runs using a 0.50 N NaCl solution at a flow rate of 389 mL/h. Wedge-shaped cell resin bed initially in the H form.

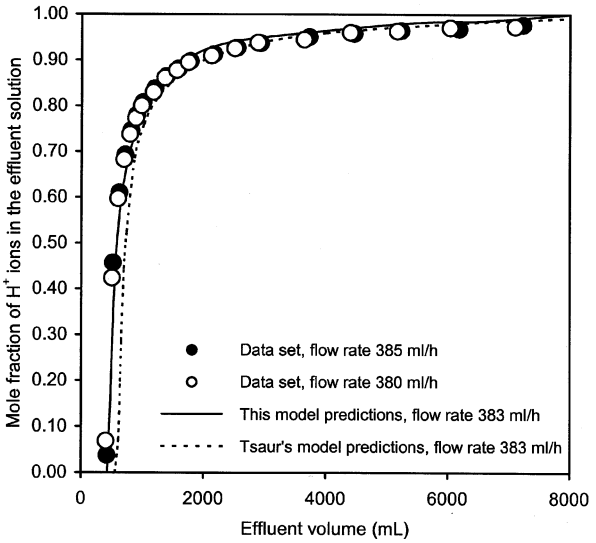

Figure 4. Breakthrough curve for the Ca−H regeneration runs using a 0.53 N HCl solution at a flow rate of 383 mL/h. Wedge-shaped cell resin bed initially in the Ca form.

the first experiment, the solution flows through at a rate of 393 mL/h, while in the second experiment, the solution flow rate is 385 mL/h. Tsaur's and the proposed models are applied using an average flow rate of 389 mL/h. The results from the two separate experiments show that data are reproducible and the agreement between the experimental observation and model prediction is excellent except for the deviation at breakthrough around 1500−1750 mL of effluent volume. In comparison with the Tsaur model, the prediction of the model proposed here is slightly better.

Figures 4 and 5 presents the breakthrough curves for the Ca−H regeneration and exhaustion cycles, respectively. As before, the proposed model gives more accurate predictions for the system performance than does the model of Tsaur and Shallcross.[5] It should be noted that neither model takes into account wall effects. The variable wall effects caused by resin beads shrinking and swelling during a resin bed under ion exchange partially lead to the derivations of the model predictions from the experimental observations. Such wall effects

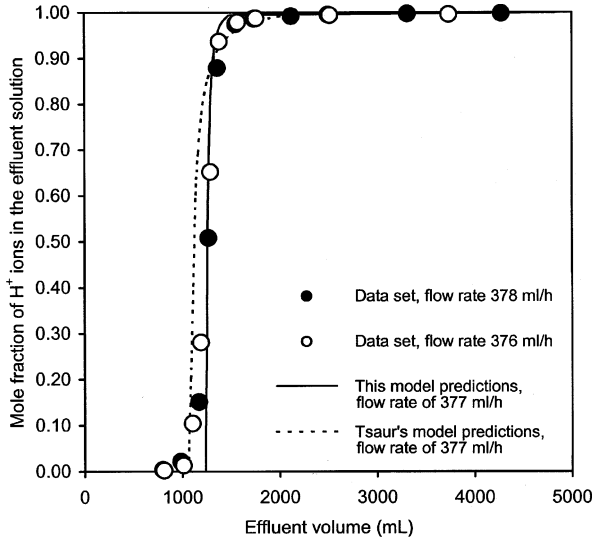

Figure 5. Breakthrough curve for the Ca−H exhaustion runs using a 0.50 N $CaCl_2$ solution at a flow rate of 377 mL/h. Wedge-shaped cell resin bed initially in the H form.

are unavoidable and are difficult to quantify independently of ion exchange.

These results effectively validate the predictions of the model proposed here for the ion-exchange performance of an annular exchange bed with radial flow.

Effects of Operating Conditions on the Ion-Exchange Performance

While the improvement in the accuracy of the predictions made by the proposed model are not dramatic, the incorporation of mass-transfer effects into the model allows the performance of the ion-exchange bed to be studied in more detail. For example, the influence of the ion-exchanger bead diameter on the system performance may be studied using the proposed model. This is not possible using the earlier model of Tsaur and Shallcross.[5,6]

Using the validated radial-flow model, computer simulations are performed to study the ion-exchange performances of an annular bed under different operating conditions, including varying bed porosities, different bed geometries, varying resin bead sizes, varying flow rates, varying injected solution concentrations, and different flow directions. The simulation results are presented and compared with respect to breakthrough time, which provides useful information on the operational efficiency of the ion-exchange processes. The simulations of the ion-exchange performance in the annular resin bed are performed within the range of the operating conditions used for the experiments to validate the models. The ion-exchange system chosen to be simulated is the Ca−H binary system because, in comparison with the Na−H binary system, the resin is highly selective.

As a base case, the operating conditions used for simulation of the ion-exchange performance in the annular resin bed are summarized in Table 5. The base case is for diverging flow, where the solution is injected at the inner face of the annular bed. The radial-flow ion-exchange model calculates the mole fractions in both the solution and resin phases at all times following injection of the feed solution. The data generated by the model simulations may be presented in different ways such as solution concentration profiles within the radial

Table 5. Base Case Simulation Parameters

initial concn in the solution phase [N]	C_0	0.50
resin bead radius [mm]	R_c	300
volumetric flow rate [L/h]	F_L	40.0
resin bed thickness [m]	H	0.50
inner radius of the resin bed [m]	R_I	0.50
outer radius of the resin bed [m]	R_O	1.00
bed volume [L]	$\pi(R_O^2 - R_I^2)H$	1178
bed porosity	ϵ_b	0.350
dispersion length [m]	λ	0.004
capacity [equiv/L of volume bed]	Q	3.94

bed at various times or the predicted effluent concentration as a function of time.

The ion-exchange performance of a bed may also be characterized by the time required for breakthrough of the exchanging ion to occur. Breakthrough may be defined as occurring when the mole fraction of contaminating ions in the effluent exceeds either 0.001 or 0.010. For the base case of the exhaustion cycle, after 265.81 h the Ca^{2+} ion mole fraction in the effluent has reached 0.001 and after 265.84 h the Ca^{2+} ion mole fraction in the effluent has risen to 0.010. However, the breakthrough of the regeneration cycle occurs very much earlier. After 21.52 h, the H^+ ion mole fraction in the effluent has risen to 0.001, and after 24.98 h, the H^+ ion mole fraction in the effluent has reached 0.010. The time difference of the breakthroughs occurring at 0.001 and 0.010 mole fractions of contaminating ions for the exhaustion cycle is small, but for the regeneration cycle, the time difference is significant. This indicates that for the exhaustion cycle the composition front remains sharp and well defined as it moves through the bed while for the regeneration cycle the composition front becomes increasingly dispersed.

Table 6 summarizes the conditions under which additional simulations of the exhaustion and regeneration cycles are performed and the ion-exchange predictions in all of the simulations expressed in terms of the breakthrough times. For almost all of the simulations, the volume of the resin bed is kept constant at 1178.1 L. In those cases in which the inner and outer bed radii vary, the volume is maintained at this constant value by varying the height of the bed. Simulations in which the ratio of the resin bed height to volume is kept constant and the resin bed height varies are also studied.

The bed performance is affected by the bed porosity. Simulations in which the bed porosity is varied between 0.30 and 0.40 are performed. For the purposes of the simulations in this study, the model assumes that the bed porosity does not vary with the change of the resin form during the ion-exchange performance cycles. As seen in Table 6, the breakthrough times for both the exhaustion and regeneration cycles increase linearly with increasing bed porosity. As the bed porosity increases, the pore velocity of the injected solution decreases. The residence time of the exchanging ions in the injection solution passing through the resin bed is longer. Hence, the breakthrough time increases with increasing bed porosity. Figure 6 presents the predictions for the regeneration ion-exchange cycles with varying bed porosity.

Simulations 4−6 study the effect of the variation of the bed's dimensions on its performance. In these runs, the bed's outer radius is held constant at 1.0 m while the inner radius is varied. In the simulations, the bed volume is kept constant by varying the bed height. It may be seen that the ion-exchange performance improves as the distance between the beds' inner and outer annular faces increases. This may be explained by the fact that, within the annular bed, the superficial velocity decreases with increasing distance from the bed's axis. As the dispersion coefficient increases with velocity, the coefficient decreases with increasing distance from the

Table 6. Summary of the Radial Simulation Conditions and Results for Exhaustion and Regeneration Runs[a]

										exhaustion runs		regeneration runs	
sim. no.	outer radius (m)	inner radius (m)	height (m)	volume (L)	flow rate (L/h)	initial concn (N)	bead radius (μm)	porosity	Péclet no. at cell	breakthrough time at 0.001 mole fraction (h)	breakthrough time at 0.010 mole fraction (h)	breakthrough time at 0.001 mole fraction (h)	breakthrough time at 0.010 mole fraction (h)
							Diverging Flow						
1	1.00	0.50	0.500	1178.1	36.0	0.50	300	0.350	250.0	265.81	265.84	21.52	24.98
2	1.00	0.50	0.500	1178.1	36.0	0.50	300	**0.300**	250.0	264.15	264.17	20.53	23.86
3	1.00	0.50	0.500	1178.1	36.0	0.50	300	**0.400**	250.0	267.49	267.52	22.50	26.11
4	1.00	**0.25**	**0.400**	1178.1	36.0	0.50	300	0.350	250.0	267.47	267.48	23.58	26.83
5	1.00	**0.75**	**0.857**	1178.1	36.0	0.50	300	0.350	250.0	261.16	261.20	17.41	21.18
6	1.00	**0.90**	**1.974**	1178.1	36.0	0.50	300	0.350	250.0	247.49	247.57	12.72	15.86
7	**0.50**	**0.25**	**2.000**	1178.1	36.0	0.50	300	0.350	125.0	264.74	264.79	18.59	22.39
8	**1.50**	**0.75**	**0.222**	1178.1	36.0	0.50	300	0.350	375.0	265.91	265.94	22.78	26.09
9	**2.00**	**1.00**	**0.125**	1178.1	36.0	0.50	300	0.350	500.0	266.08	266.09	23.55	26.76
10	1.00	0.50	**0.250**	**589.1**	36.0	0.50	300	0.350	250.0	132.97	132.99	10.71	12.46
11	1.00	0.50	**0.750**	**1767.2**	36.0	0.50	300	0.350	250.0	398.61	398.64	32.32	37.55
12	1.00	0.50	**1.000**	**2356.2**	36.0	0.50	300	0.350	250.0	531.38	531.43	43.16	50.09
13	1.00	0.50	0.500	1178.1	36.0	0.50	**100**	0.350	250.0	266.26	266.28	22.04	25.40
14	1.00	0.50	0.500	1178.1	36.0	0.50	**200**	0.350	250.0	266.04	266.06	21.78	25.20
15	1.00	0.50	0.500	1178.1	36.0	0.50	**400**	0.350	250.0	265.37	265.37	21.24	24.77
16	1.00	0.50	0.500	1178.1	**24.0**	0.50	300	0.350	250.0	398.61	398.64	32.32	37.55
17	1.00	0.50	0.500	1178.1	**48.0**	0.50	300	0.350	250.0	199.40	199.42	16.10	18.73
18	1.00	0.50	0.500	1178.1	**60.0**	0.50	300	0.350	250.0	159.55	159.56	12.87	14.96
19	1.00	0.50	0.500	1178.1	36.0	**0.10**	300	0.350	250.0	824.46	824.48	24.98	29.42
20	1.00	0.50	0.500	1178.1	36.0	**0.25**	300	0.350	250.0	567.41	567.44	23.60	27.62
21	1.00	0.50	0.500	1178.1	36.0	**1.00**	300	0.350	250.0	138.16	138.18	18.14	21.03
							Converging Flow						
22	1.00	0.50	0.500	1178.1	36.0	0.50	300	0.350	250.0	264.13	264.14	20.87	24.23
23	**0.50**	**0.25**	**2.000**	1178.1	36.0	0.50	300	0.350	125.0	262.10	262.13	17.90	21.53
24	**1.50**	**0.75**	**0.222**	1178.1	36.0	0.50	300	0.350	375.0	264.71	264.73	22.17	25.37
25	**2.00**	**1.00**	**0.125**	1178.1	36.0	0.50	300	0.350	500.0	265.28	265.29	22.95	26.06

[a] Bold entries indicate changed values with respect to the base case.

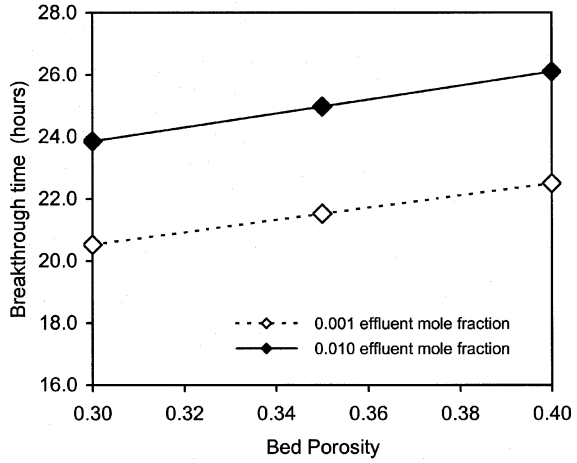

Figure 6. Effects of varying the bed porosity on the predicted ion-exchange performance of the regeneration cycles as indicated by breakthrough times for an annular bed of the base case dimensions. Diverging flow.

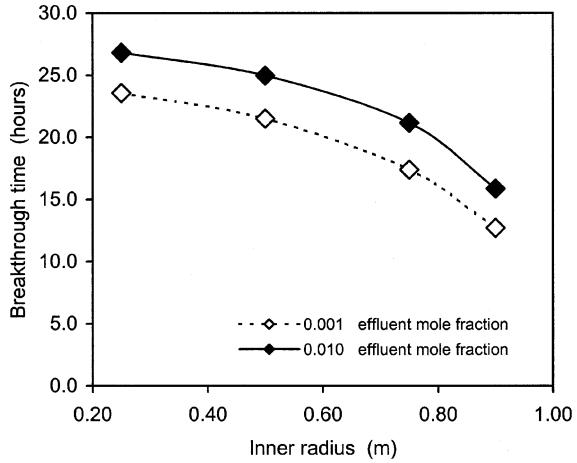

Figure 7. Predicted ion-exchange performance of the regeneration cycles as indicated by breakthrough times for an annular bed of a constant outer radius of 1.00 m but varying inner radius. The bed volume remains constant by varying the bed height. Diverging flow.

axis. Thus, the rate at which dispersion grows within the annular bed slows as the solution moves away from the bed's axis. As a result, the breakthrough times for the exhaustion and regeneration cycles occur earlier as the travel distance of the injected solution decreases. Figure 7 presents the ion-exchange performance for the regeneration cycles as indicated by breakthrough times for an annular bed.

Simulations 7−9 study the bed's performance when the bed's inner and outer radii are varied while their ratio is held constant. In these simulations, $R_o/R_i = 2.00$ and the bed volume is kept constant by varying the bed height. Figure 8 presents the ion-exchange performance of the regeneration cycles as indicated by breakthrough times for these simulations. The results of the simulations show that the ion-exchange performance of the exhaustion and regeneration cycles improves with increasing radius. Again the results are accounted for by the increase in the distance between the inner and outer faces of the bed. The further the solution must travel within the bed, the better the performance.

A further series of simulations (10−12) are performed in which the ratio of the resin bed height to the bed volume is kept constant, while the resin bed height is varied. As expected, the breakthrough times for both

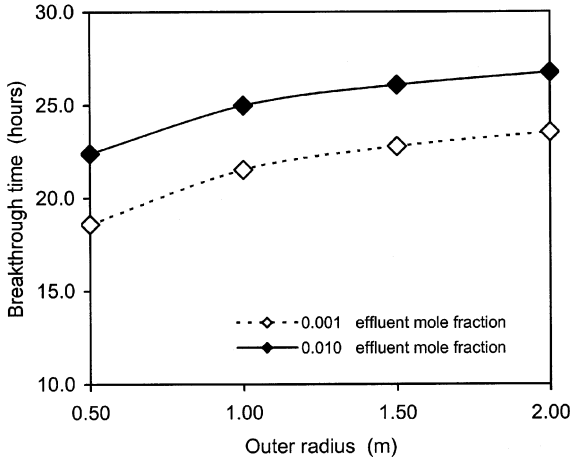

Figure 8. Predicted ion-exchange performance of the regeneration cycles as indicated by breakthrough times for an annular bed with $R_o/R_i = 2.000$. The bed height varies, and the bed volume remains constant. Diverging flow.

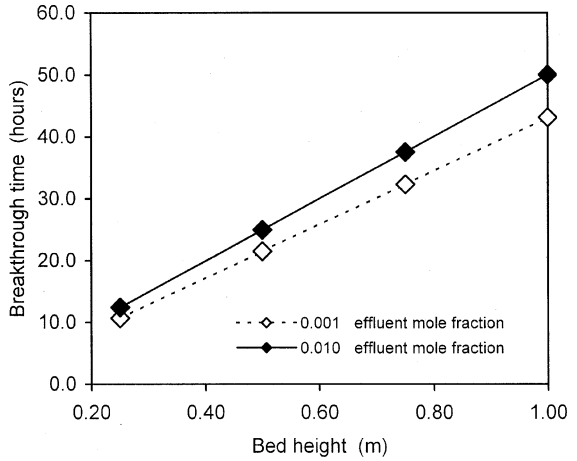

Figure 9. Predicted ion-exchange performance of the regeneration cycles as indicated by breakthrough times for an annular bed with H/V_{bed} = constant. The bed height varies. Diverging flow.

the exhaustion and regeneration cycles increase when the resin bed height increases. The higher the resin bed height, the greater the cross-sectional area of the bed perpendicular to flow, the lower the velocity of the injected solution, and the higher the breakthrough time. Figure 9 presents the ion-exchange performance for the regeneration cycles as indicated by breakthrough times for an annular bed.

All of the previous simulations are conducted with the spherical exchanger beads having a uniform radius of 300 μm. Simulations 13−15 study the effect of varying the resin bead size on the system performance. Figure 10 presents the results. As shown, increasing the resin bead sizes causes the breakthrough times of both the exhaustion and regeneration cycles to decrease slightly as expected. The resin bed is assumed to be packed uniformly and the bed porosity is assumed to be constant during the ion-exchange cycles. As the surface area of the resin bed increases with decreasing resin bead sizes, the interchange of the ions in the solution and exchanger phases increases. Consequently, the breakthrough times for both the exhaustion and regeneration cycles increase with decreasing exchanger bead diameter.

The flow rate of the injected solution is varied in simulations 16−18. The results are presented in Figure 11. As expected, higher flow rates cause a noticeably

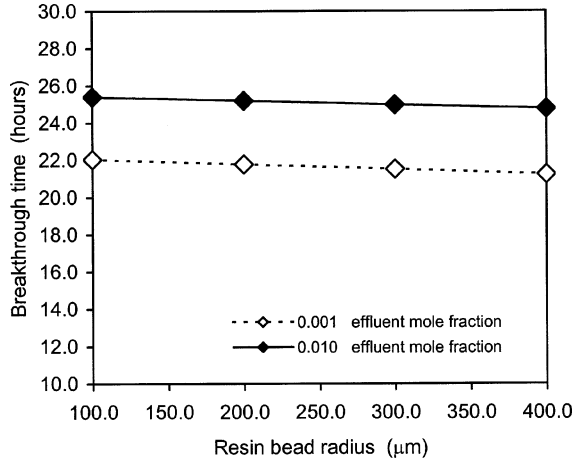

Figure 10. Effects of varying the resin bead sizes on the predicted ion exchange of the regeneration cycles as indicated by breakthrough times for an annular bed of the base case dimensions. Diverging flow.

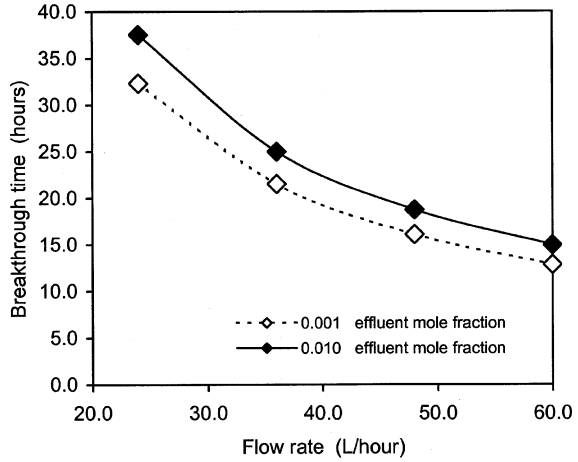

Figure 11. Effects of varying the flow rates on the predicted ion exchange of the regeneration cycles as indicated by breakthrough times for an annular bed of the base case dimensions. Diverging flow.

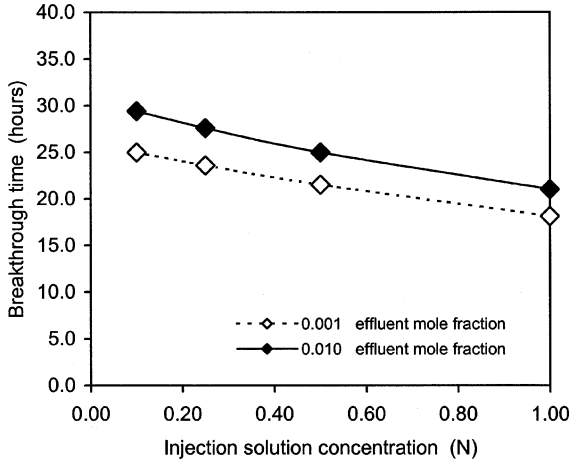

Figure 12. Effects of varying the injected solution concentrations on the predicted ion exchange of the regeneration cycles as indicated by breakthrough times for an annular bed of the base case dimensions. Diverging flow.

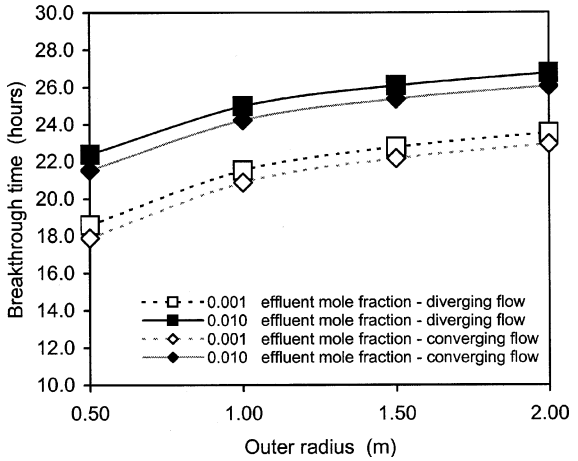

Figure 13. Effects of diverging and converging flow on the predicted ion-exchange performance of the regeneration cycles as indicated by breakthrough times for an annular bed with $R_o/R_i = 2.000$. The bed height varies, and the bed volume remains constant.

earlier breakthrough for both the exhaustion and regeneration cycles. Under the same operation conditions, the higher the flow rate of the injected solution increases, the less time the exchanging ions remain in the resin bed and the earlier the breakthrough times of the exhaustion and regeneration cycles occur. Consequently, increasing the flow rate reduces marginally the capacity in the annular cell.

The effect of varying the injected solution concentration on the system performance is studied in simulations 19−22. The predictions are presented in Figure 12. As expected, the higher the solution concentration, the faster the bed changes form.

To study the influence of the direction of flow through the annular bed, simulations 22−25 are presented. Simulation 22 is identical with the base case except that the solution converges toward the axis rather than diverging away from it. The additional simulations were performed for varying bed radii but with $R_o/R_i = 2.00$. The results are presented in Figure 13. In all cases under similar operating conditions, breakthrough in converging flow for both the exhaustion and regeneration cycles occurs earlier than that in the corresponding diverging-flow simulations. Because the superficial velocity increases with decreasing radial distance in converging flow as the solution moves toward the bed's axis, dispersion increases. The growth rate of the dispersion for the converging flow may be higher than that for diverging flow. Therefore, the breakthrough of the exhaustion and regeneration cycles for converging flow occurs earlier than that for diverging flow.

Concluding Remarks

A mathematical model is developed to predict the ion-exchange performance in an annular ion-exchange bed. By incorporation of mass-transfer effects and by the elimination of the assumption of instantaneous equilibrium throughout the bed, the model is a significant improvement over the existing model. The proposed model predicts well the radial-flow ion-exchange performance in a wedge-shaped cell and more accurately than the existing model of Tsaur and Shallcross.[5] The proposed radial-flow ion-exchange model may be used to predict the radial-flow ion-exchange performance of both the exhaustion and regeneration runs over a wide range of flow rates of the injected solution and solution concentrations without any model modification. The proposed model for the ion-exchange performance of an

annular bed is a powerful design tool for the design of annular ion-exchange beds.

Nomenclature

a = valence of the A cation
a_s = surface area, m^2
A_R = annular cross-sectional area, m^2
b = valence of the B cation
$\bar{C}_A$ = solution-phase concentration of A cations at the interface surface, mol/m^3
C_0 = total normality in the solution, mol/m^3
C_i = concentration of i cations in the solution phase, mol/m^3
C_{Ri} = concentration of i cations in the solid-exchanger phase, mol/m^3
D_{LR} = radial dispersion coefficient for nonlinear flow, m^2/s
F_L = volumetric rate, m^3/s
H = thickness of the annular bed, m
J_i = dispersion flux of i cations in solution, mol/s·m
k = penal power of the weighting function
k_f = mass-transfer coefficient, m/s
N = number of experimental data
p_1-p_6 = empirical constants of the equilibrium isotherm equation
Pe_R = Péclet number for nonlinear flow
Q_c = cation-exchanger capacity of the resin on a mass basis, mol/kg
Q_{RT} = total exchange capacity of the annular exchanger bed, mol
r = dimensionless radial position
r_p = radial distance from the center of the particle, m
R = radial distance from the central inlet, m
R_c = resin bead radius, m
R_I = inlet radius of the annular bed, m
R_O = outlet radius of the annular bed, m
$\mathscr{R}$ = weighted relative residue
U_{LP} = pore velocity for linear flow, m/s
U_R = superficial velocity for nonlinear flow, m/s
U_{RP} = radial pore velocity for nonlinear flow, m/s
V_{bed} = resin bed volume, m^3
$V_{experiment}$ = effluent volume of the experiment, m^3
$V_{predict}$ = effluent volume of model prediction, m^3
V_R = variable volume of the exchanger bed, m^3
W = weighting function
t = dimensionless time
x = solution phase mole fraction
$\bar{x}$ = surface mole fraction in solution in equilibrium with the resin phase mole fraction
y = resin phase mole fraction
z = dimensionless axial position
ϵ_b = resin bed porosity
ρ_c = resin density, kg/m^3
τ = time, s
υ = volume of a spherical cation resin bead, m^3

Literature Cited

(1) Schneider, H. M.; Allen, E.; Woodling, R.; Barnes, R. Method for Removing Contaminants from Water. U.S. Patent 5,597,489, Jan 28, 1997.

(2) Dorfner, K. *Ion exchangers*; Walter de Gruyter: Berlin, 1991.

(3) Slater M. J. *Principle of Ion Exchange Technology*; Butterworth-Linacre: Oxford, U.K., 1991.

(4) Koh, J. H.; Wankat, P. C.; Wang, N. H. L. Pore and Surface Diffusion and Bulk-Phase Mass Transfer in Packed and Fluidized Beds. *Ind. Eng. Chem. Res.* **1998**, *37*, 228−239.

(5) Tsaur, Y.; Shallcross, D. C. Modeling of Ion Exchange Performance in a Fixed Radial Flow Annular Bed. *Ind. Eng. Chem. Res.* **1997**, *36*, 2359−2367.

(6) Tsaur, Y.; Shallcross D. C. Comparison of Simulated Performance of Fixed Ion Exchange Beds in Linear and Radial Flow. *Solvent Extr. Ion Exch.* **1997**, *15* (4), 689−708.

(7) Rachinskii, V. V. Basic Principles of Radial Chromatography. *J. Chromatogr.* **1968**, *33*, 234−241.

(8) Hang, S. H.; Lee, W. C.; Tsao, G. T. Mathematical Models for Radial Chromatography. *Chem. Eng. J.* **1988**, *38*, 179−186.

(9) Rice, R. G.; Heft, B. K. Separations via Radial Flow Chromatography in Compacted Particle Beds. *AIChE J.* **1991**, *37*, 629−632.

(10) Tan, C. T.; Homsy, G. M. Stability of Miscible Displacements in Porous Media. *Phys. Fluid* **1987**, *30*, 1239−1245.

(11) Yortsos, Y. C. Dispersion Driven Instability in Miscible Displacement in Porous Media. *Phys. Fluid* **1988**, *31*, 3511−3518.

(12) Zimmerman, W. B.; Homsy, G. M. Nonlinear Viscous Fingering in Miscible Displacement with Anisotropic Dispersion. *Phys. Fluid* **1991**, *3*, 1858−1872.

(13) Mehablia, M. A.; Shallcross, D. C.; Stevens, G. W. Prediction of Multicomponent Ion Exchange Equilibria. *Chem. Eng. Sci.* **1994**, *49* (14), 2277−2286.

(14) Mehablia, M. A.; Shallcross, D. C.; Stevens, G. W. Prediction of Ion Exchange Equilibria for the $H^+-Na^+-K^+$ and $H^+-Na^+-K^+-Ca^{2+}$ Systems. *Solvent Extr. Ion Exch*. **1996**, *14* (2), 309−322.

(15) Duong, H. M. Modeling radial ion exchange processes incorporating mass transfer phenomena. Ph.D. Thesis, University of Melbourne, Melbourne, Australia, 1994.

(16) Tsaur, Y. Radial Ion Exchange Processes. Ph.D. Thesis, University of Melbourne, Melbourne, Australia, 1997.

Received for review November 2, 2004
Revised manuscript received February 20, 2005
Accepted March 1, 2005

IE048941Y